Marine Technology and Engineering – Guedes Soares et al. (Eds)
© 2011 Taylor & Francis Group, London, ISBN 978-0-415-69808-5

A sophisticated beam model for hydroelastic analysis of Ultra Large Container Ships

I. Senjanović, N. Vladimir & M. Tomić
University of Zagreb, Faculty of Mechanical Engineering and Naval Architecture, Croatia

Š. Malenica
Bureau Veritas, Marine Division, France

ABSTRACT: A numerical procedure for hydroelastic analysis of Ultra Large Container Ships (ULCS) which utilizes sophisticated beam model coupled with 3D BEM hydrodynamic model, has been summarized. Beside general description of the methodology for ship hydroelastic analysis and constitutive parts of the hydroelastic mathematical model, special attention is paid to several improvements of the beam structural model. The first one is related to derivation of finite element for coupled beam horizontal and torsional vibrations, with influence of shear on both bending and torsion. The second improvement includes contribution of transverse bulkheads to the hull torsional stiffness, based on theory of thin-walled girders and orthotropic plate theory, while the third one is related to an appropriate incorporating of the relatively short closed engine room segment into the beam model. The significance of theoretical considerations is confirmed within two numerical examples. The first example includes complete hydroelastic analysis of a 7800 TEU container ship, and in that particular case 1D FEM model is checked by correlation analysis with the vibration response of the fine 3D FEM model. The procedure related to the determination of the engine room effective stiffness is verified within the second numerical example, by 3D FEM analysis of ship-like pontoon.

1 INTRODUCTION

Modern sea transport requires design and building of Ultra Large Container Ships (ULCS), which are relatively flexible and fast vessels and their natural frequencies could fall into the range of encounter frequencies in an ordinary sea spectrum. Such conditions are not covered by present Rules and direct calculations are required to ensure ship safety.

The classical theories for determination of ship motions and wave loads, as for example (Salvesen et al., 1970), are based on the assumption that the ship hull is a rigid body. Usually, the wave load obtained according to these theories is imposed to the elastic 3D FEM model of ship structure in order to analyze global strength, as well as local strength with stress concentrations related to fatigue. Although the above approach is good enough for ships with closed cross-section and ordinary hatch openings such as tankers, bulk carriers or general cargo ships, it is not reliable as it should be for ultra large container ships due to mutual influence of the wave load and structure response (Senjanović et al., 2009a, 2010). Therefore, a more reliable solution requires analysis of wave load and ship vibration as a coupled hydroelastic problem (Bishop & Price, 1979). This is very important for impulsive loads such as ship slamming and slamming induced whipping.

Numerical procedure for ship hydroelastic analysis requires definition of structural model, ship and cargo mass distributions, and geometrical model of ship wetted surface (Senjanović et al., 2007, 2008a, 2009b, 2010).

In this paper, the emphasis is given on structural model based on the beam and thin-walled girder theories for calculation of dry natural vibrations of container ships, as an important step in their hydroelastic analysis (Senjanović et al., 2009c). Basic structural model is described in (Tomašević, 2007), and here its improvements are given. First improvement is related to taking into account shear influence on torsion as an extension of shear influence on bending (Pavazza, 2005). The second one includes contribution of transverse bulkheads to hull stiffness (Senjanović et al., 2008b). Third improvement is related to influence of engine room structure on hull stiffness of ULCS, and it is considered in details in separate chapter. Apart from that, methodology of ship hydroelastic analysis is briefly illustrated. Also, short description of hydrostatic and hydrodynamic submodels, and hydroelastic model is given. Applied numerical procedure as well as developed computer codes is

verified. Finally, the results of hydroelastic analysis of 7800 TEU container ship are shown. It should be mentioned that the verification of applied numerical procedure is done by correlation analysis of the simulation results and the measured ones for a flexible segmented barge, for which test results are available (Malenica et al., 2003, 2007, Remy et al., 2006). Details of the verification are shown in (Senjanović et al., 2009a, 2010, Tomašević, 2007).

2 METHODOLOGY OF SHIP HYDROELASTIC ANALYSIS

As mentioned above, structural model, ship and cargo mass distributions and geometrical model of ship surface have to be defined to perform ship hydroelastic analysis. At the beginning, dry natural vibrations have to be calculated, and after that modal hydrostatic stiffness, modal added mass, damping and modal wave load are determined. Finally, wet natural vibrations as well as the transfer functions (RAO) for determining ship structural response to wave excitation are obtained (Senjanović et al., 2008a, 2009b).

3 STRUCTURAL MODEL DESCRIPTION

3.1 *General*

A ship hull, as an elastic non-prismatic thin-walled girder, performs longitudinal, vertical, horizontal and torsional vibrations. Since the cross-sectional centre of gravity and centroid, as well as the shear centre positions are not identical, coupled longitudinal and vertical, and horizontal and torsional vibrations occur, respectively. The shear centre in ships with large hatch openings is located below the keel and therefore the coupling of horizontal and torsional vibrations is extremely high. The above problem is rather complex due to geometrical discontinuity of the hull cross-section, Figure 2.

The accuracy of the solution depends on the reliability of stiffness parameters determination, i.e., of bending, shear, torsional and warping moduli. The finite element method is a powerful tool to solve the above problem in a successful way. One of the first solutions for coupled horizontal and torsional hull vibrations, dealing with the finite element technique, is given in (Kawai, 1973, Senjanović & Grubišić, 1991). Generalised and improved solutions are presented in (Pedersen, 1985, Wu & Ho, 1987). In all these references, the determination of hull stiffness is based on the classical thin-walled girder theory, which doesn't give a satisfactory value for the warping modulus of the open cross-section (Haslum & Tonnessen, 1972, Vlasov, 1961). Apart from that, the fixed values of stiffness moduli are determined, so that the application of the beam theory for hull vibration analysis is limited to a few lowest natural modes only. Otherwise, if the mode dependent stiffness parameters are used the application of the beam theory can be extended up to the tenth natural mode (Senjanović & Fan, 1989, 1992, 1997).

3.2 *An advanced beam theory*

Referring to the Timoshenko's flexural beam theory, the total beam deflection, w, consists of the bending deflection, w_b, and the shear deflection, w_s, i.e., (Senjanović & Grubišić, 1991), Figure 2

$$w = w_b + w_s. \tag{1}$$

The shear deflection is a function of w_b

$$w_s = -\frac{EI_b}{GA_s}\frac{\partial^2 w_b}{\partial x^2}, \tag{2}$$

where E and G are the Young's and shear modulus, respectively, while I_b, and A_s are the

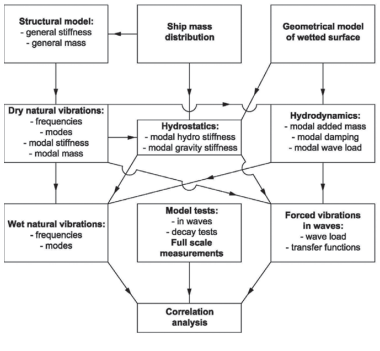

Figure 1. Methodology of the hydroelastic analysis.

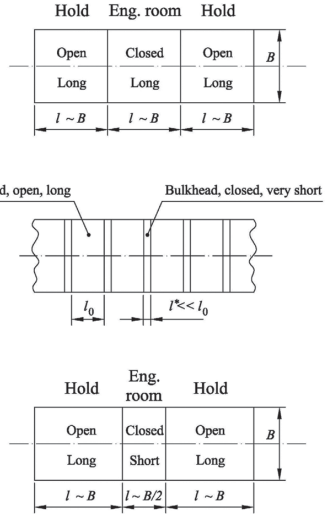

Figure 2. Discontinuities of ship hull.

moment of inertia of cross-section and shear area, respectively. The angle of cross-section rotation is caused by the bending deflection

$$\varphi = \frac{\partial w_b}{\partial x}. \tag{3}$$

The cross-sectional forces are the bending moment and the shear force

$$M = -EI_b \frac{\partial^2 w_b}{\partial x^2}, \tag{4}$$

$$Q = GA_s \frac{\partial w_s}{\partial x} = -EI_b \frac{\partial^3 w_b}{\partial x^3}. \tag{5}$$

Concerning torsion, the total twist angle, ψ, consists of the pure twist angle, ψ_t, and the shear contribution, ψ_s, i.e., Figure 3

$$\psi = \psi_t + \psi_s. \tag{6}$$

Referring to the analogy of torsion and bending (Pavazza, 2005), the shear angle depends on the twist angle, similarly to Eq. (2)

$$\psi_s = -\frac{EI_w}{GI_s} \frac{\partial^2 \psi_t}{\partial x^2}, \tag{7}$$

where I_w is the warping modulus and I_s is the shear inertia modulus. The second beam displacement, which causes warping of cross-section (similarly to the cross-section rotation due to bending) is a variation of the pure twist angle

$$\vartheta = \frac{\partial \psi_t}{\partial x}. \tag{8}$$

The sectional forces include the total torque, T, which consists of pure torsional torque, T_t, and the warping torque T_w i.e.,

$$T = T_t + T_w, \tag{9}$$

where

$$T_t = GI_t \frac{\partial \psi_t}{\partial x} \tag{10}$$

$$T_w = GI_s \frac{\partial \psi_s}{\partial x} = -EI_w \frac{\partial^3 \psi_t}{\partial x^3} \tag{11}$$

and the bimoment given by

$$B_w = EI_w \frac{\partial^2 \psi_t}{\partial x^2}. \tag{12}$$

1D FEM procedure for vertical ship hull vibrations is well known in literature, while coupled horizontal and torsional vibrations are a more complex problem. Due to analogy between bending and torsion the same shape functions, represented by Hermitian polynomials, are used. The matrix finite element equation for coupled vibration yields (Senjanović, 1998)

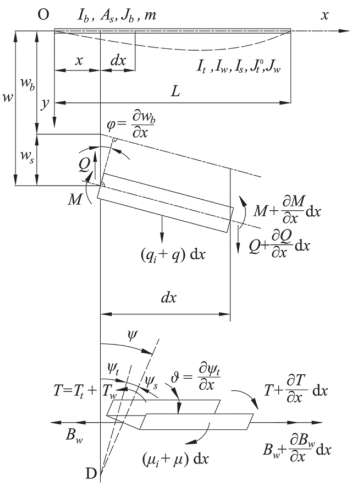

Figure 3. Beam bending and torsion.

$$\mathbf{f^e} = \mathbf{k^e}\boldsymbol{\delta}^\mathbf{e} + \mathbf{m^e}\ddot{\boldsymbol{\delta}}^\mathbf{e}, \tag{13}$$

where $\mathbf{f^e}$ is nodal forces vector, $\boldsymbol{\delta}^\mathbf{e}$ is nodal displacements vector, $\mathbf{k^e}$ is stiffness matrix, and $\mathbf{m^e}$ is mass matrix. These quantities consist of flexural and torsional parts

$$\mathbf{f^e} = \begin{Bmatrix} \mathbf{P} \\ \mathbf{R} \end{Bmatrix}, \quad \boldsymbol{\delta}^\mathbf{e} = \begin{Bmatrix} \mathbf{U} \\ \mathbf{V} \end{Bmatrix} \tag{14}$$

$$\mathbf{k^e} = \begin{bmatrix} \mathbf{k_{bs}} & 0 \\ 0 & \mathbf{k_{wt}} \end{bmatrix}, \quad \mathbf{m^e} = \begin{bmatrix} \mathbf{m_{sb}} & \mathbf{m_{st}} \\ \mathbf{m_{ts}} & \mathbf{m_{tw}} \end{bmatrix}. \tag{15}$$

Vectors of nodal forces and displacements are

$$\mathbf{P} = \begin{Bmatrix} -Q(0) \\ M(0) \\ Q(l) \\ -M(l) \end{Bmatrix}, \quad \mathbf{R} = \begin{Bmatrix} -T(0) \\ -B_w(0) \\ T(l) \\ B_w(l) \end{Bmatrix} \tag{16}$$

$$\mathbf{U} = \begin{Bmatrix} w(0) \\ \varphi(0) \\ w(l) \\ \varphi(l) \end{Bmatrix}, \quad \mathbf{V} = \begin{Bmatrix} \psi(0) \\ \vartheta(0) \\ \psi(l) \\ \vartheta(l) \end{Bmatrix}. \tag{17}$$

In the above formulae symbols Q, M, T and B_w denote shear force, bending moment, torque and warping bimoment, respectively. Also, w, φ, ψ and ϑ are deflection, rotation of cross-section,

twist angle and its variation, respectively. The submatrices, which are specified in (Senjanović et al., 2009c), have the following meanings:

k_{bs} – bending—shear stiffness matrix
k_{wt} – warping—torsion stiffness matrix
m_{sb} – shear—bending mass matrix
m_{tw} – torsion—warping mass matrix
$m_{st} = m_{ts}^T$ – shear—torsion mass matrix.

It is obvious that coupling between horizontal and torsional vibrations is realized through the mass matrix due to eccentricity of the centre of gravity and shear centre.

Before assembling of finite elements it is necessary to transform Eq. (13) in such a way that all the nodal forces as well as nodal displacement, Eqs. (16) and (17), are related to the first and then to the second node. Furthermore, Eq. (13) has to be transformed from local to global coordinate system. The origin of the former is located at the shear centre, and of the latter at the base line.

3.3 *Contribution of transverse bulkheads*

This problem for container ships is extensively analyzed in (Senjanović et al., 2008b), where torsional modulus of ship cross-section is increased proportionally to the ratio of bulkhead strain energy and strain energy of hull portion. The bulkhead is considered as an orthotropic plate with very strong stool (Szilard, 2004). Bulkhead strain energy is determined for the given warping of cross-section as a boundary condition. The warping causes bulkhead screwing and bending. Here, only the review of the final results is presented. Bulkhead deflection (axial displacement) is given by the following formula, Figure 4:

$$u(y,z) = -y\left\{(z-d) + \left[1-\left(\frac{y}{b}\right)^2\right]\frac{z^2}{H}\left(2-\frac{z}{H}\right)\right\}\psi', \qquad (18)$$

where H is the ship height, b is one half of bulkhead breadth, d is the distance of warping centre from double bottom neutral line, y and z are transverse and vertical coordinates, respectively, and ψ' is the variation of twist angle.

The bulkhead grillage strain energy includes vertical and horizontal bending with contraction, and torsion (Senjanović et al., 2008b).

$$U_g = \frac{1}{1-\nu^2}\left[\frac{116H^3}{35b}i_y + \frac{32b^3}{105H}i_z + \frac{8Hb}{75}\nu\left(i_y+i_z\right) + \frac{143Hb}{75}(1-\nu)i_t\right]E\psi'^2 \qquad (19)$$

where i_y, i_z and i_t are the average moments of inertia of cross-section and torsional modulus per unit breadth, respectively. The stool strain energy

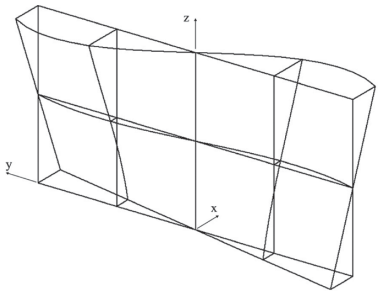

Figure 4. Shape of bulkhead deformation.

is comprised of the bending, shear and torsional contributions

$$U_s = \left[\frac{12h^2 I_{sb}}{b} + 72(1+\nu)\frac{h^2}{b^3}\frac{I_{sb}^2}{A_s} + \frac{9bI_{st}}{10(1+\nu)}\right]E\psi'^2 \qquad (20)$$

where I_{sb}, A_s and I_{st} are the moment of inertia of cross-section, shear area and torsional modulus, respectively. Quantity h is the stool distance from the inner bottom, Figure 5.

The equivalent torsional modulus yields, Figure 5

$$I_t^* = \left[1 + \frac{a}{l_1} + \frac{4(1+\nu)C}{I_t l_0}\right]I_t, \qquad (21)$$

where a is the web height of bulkhead girders (frame spacing), l_0 is the bulkhead spacing, $l_1 = l_0 - a$ is the net length, and C is the energy coefficient

$$C = \frac{U_g + U_s}{E\psi'^2}. \qquad (22)$$

The second term in (21) is the main contribution of the bulkhead as the closed cross-section segment of ship hull, and the third one comprises the bulkhead strain energy.

3.4 *Natural vibration analysis*

If the FEM approach is used, the governing equation of dry natural vibrations yields (Bathe, 1996)

$$\left(\mathrm{K} - \Omega^2\mathrm{M}\right)\boldsymbol{\delta} = \mathbf{0}, \qquad (23)$$

where $\mathbf{K}$ is stiffness matrix, $\mathbf{M}$ is mass matrix, Ω is dry natural frequency and $\boldsymbol{\delta}$ is dry natural mode. As solution of the eigenvalue problem (23) Ω_i and $\boldsymbol{\delta}_i$ are obtained for each the i-th dry mode, where $i = 1, 2 \ldots N$, N is total number of degrees of freedom. Now natural modes matrix can be constituted

$$\delta = \left[\delta_1, \delta_2 \ldots \delta_i \ldots \delta_N\right] \qquad (24)$$

and the modal stiffness and mass can be determined (Senjanović, 1998)

$$\mathrm{k} = \delta^T \mathrm{K}\, \delta, \quad \mathrm{m} = \delta^T \mathrm{M}\, \delta. \tag{25}$$

Since the dry natural vectors are mutually orthogonal, matrices **k** and **m** are diagonal. Terms k_i and $\Omega_i^2 m_i$ represent strain and kinetic energy of the *i*-th mode respectively.

Generally the first six natural frequencies Ω_i are zero with corresponding eigenvectors representing the rigid body modes. As a result, the first six diagonal elements of **k** are also zero, while the first three elements in **m** are equal to structure mass, the same in all directions *x*, *y*, *z*, and the next three elements represent the mass moment of inertia around the corresponding coordinate axes.

If 1D analysis is applied, the beam modes are spread to the ship wetted surface using the expressions for vertical vibrations (Senjanović et al., 2009a)

$$\mathbf{h}_i = -\frac{\mathrm{d}\, w_{vi}}{\mathrm{d}\, x}(z - z_N)\mathbf{i} + w_{vi}\mathbf{k}, \tag{26}$$

and for coupled horizontal and torsional vibrations

$$\begin{aligned}\mathbf{h}_i = &\left(-\frac{\mathrm{d}\, w_{hi}}{\mathrm{d}\, x}\, y + \frac{\mathrm{d}\, \psi_i}{\mathrm{d}\, x}\, \bar{u}\right)\mathbf{i} \\ &+ \left[w_{hi} + \psi_i (z - z_S)\right]\mathbf{j} - \psi_i\, y\, \mathbf{k},\end{aligned} \tag{27}$$

where *w* is hull deflection, ψ is twist angle, *y* and *z* are coordinates of the point on ship surface, and z_N and z_S are coordinates of centroid and shear centre respectively, and $\bar{u} = \bar{u}(x, y, z)$ is the cross-section warping intensity reduced to the wetted surface (Senjanović et al., 2009d).

4 CONTRIBUTION OF ENGINE ROOM STRUCTURE TO HULL STIFFNESS

Ultra Large Container Ships are characterized by relatively short engine room structure with length of about a half of ship breadth, Figure 2. Its complex deformation is illustrated in a case of a 11400 TEU container ship, Figure 6. The deck shear deformation is predominant, while hold transverse bulkhead stool is exposed to bending. Due to shortness of the engine room, its transverse bulkheads are skewed but somewhat less pronounced than warping of the hold bulkheads. Warping of the transom is negligible, and that is an important fact when specifying boundary conditions in vibration analysis.

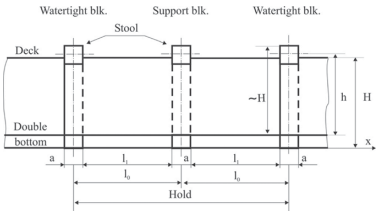

Figure 5. Longitudinal section of container ship hold.

4.1 *Stiffness of engine room structure*

A short engine room structure can be considered either as a closed segment with relevant stiffness or as an open segment with increased stiffness due to deck contribution (Pedersen, 1985). The latter simulation in fact gives results which agree better with FEM results, than the former one (Pedersen, 1983). Indeed, 3D FEM analysis shows that a short engine room structure behaves similar to an open one with shear centre being moved from inside of cross-section below the keel and quite close to that of open hold structure. In that way coupling between torsion and horizontal bending through twist angle ψ and shear force Q is negligible.

Deck contribution to hull stiffness can be determined by energy approach, as it is done in the case of transverse bulkheads (Senjanović et al., 2008b). Such a beam model is consistent at global level of energy balance, and that is sufficient for application in ship hydroelastic analysis, where proper natural frequencies and mode shapes of dry hull are required.

In the case of short engine room, torsion induces distortion of cross-section while hull bending is negligible. Solution of that complex problem is described here by employing the energy balance approach and concept of the effective stiffness due to reason of simplicity. A closed hull segment is considered as open one with deck influence. For that purpose let us determine deck strain energy. All quantities related to closed and open cross-section are designated by $(.)^*$ and $(.)^\circ$, respectively

As it can be seen in Figure 6, the upper deck is exposed to large deformation, while the double bottom in-plane deformation is quite small. The relative axial displacement of the internal upper deck boundaries, with respect to double bottom, is result of their warping

$$U = |U_D| + |U_B| = \left(|w_D| + |w_B|\right)\psi_i' \tag{28}$$

It causes deck in-plane (membrane) deformation. The problem can be solved in an approximate analytical way by considering deck as a beam. Its horizontal anti-symmetric deflection consists of pure bending and shear contribution, Figure 7. The former is assumed in the form

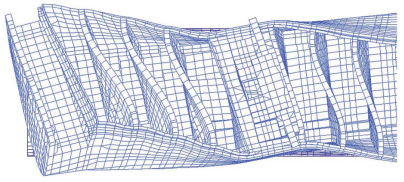

Figure 6. 11400 TEU container ship aft structure.

$$u_b = \frac{y}{2b}\left[3-\left(\frac{y}{b}\right)^2\right]U_b, \tag{29}$$

which satisfies relevant boundary conditions: $u_b(0)=0$ and $u_b''(0)=0$, where U_b is the boundary bending deflection. Shear deflection depends on bending deflection

$$u_s = -\frac{EI}{GA}\frac{\mathrm{d}^2u_b}{\mathrm{d}y^2} = 2(1+\nu)\left(\frac{a}{b}\right)^2\frac{y}{b}U_b, \tag{30}$$

where the internal deck cross-section area, $A=2at$, its moment of inertia, $I=\frac{2}{3}a^3t$, and the relation $E=2(1+\nu)G$, are taken into account, Figure 7. Total deflection is obtained by summing up Eqs. (29) and (30), i.e., $u=u_b+u_s$. Relation between total boundary deflection and the bending boundary deflection reads

$$U=\left[1+2(1+\nu)\left(\frac{a}{b}\right)^2\right]U_b \tag{31}$$

The total internal deck strain energy consists of the bending and shear contributions

$$E_1=\frac{1}{2}EI\int_{-b}^{b}\left(\frac{\mathrm{d}^2u_b}{\mathrm{d}y^2}\right)^2\mathrm{d}y+\frac{1}{2}GA\int_{-b}^{b}\left(\frac{\mathrm{d}u_s}{\mathrm{d}y}\right)^2\mathrm{d}y \tag{32}$$

By substituting Eqs. (29) and (30) into (32), one finds

$$E_1=\frac{1}{2}EI\int_{-b}^{b}\left(\frac{\mathrm{d}^2u_b}{\mathrm{d}y^2}\right)^2\mathrm{d}y+\frac{1}{2}GA\int_{-b}^{b}\left(\frac{\mathrm{d}u_s}{\mathrm{d}y}\right)^2\mathrm{d}y \tag{32}$$

Finally, by taking into account Eqs. (28) and (31), yields

$$E_1=\frac{4(1+\nu)Gt\left(\frac{a}{b}\right)^3}{1+2(1+\nu)\left(\frac{a}{b}\right)^2}\left(|w_D|+|w_B|\right)^2\psi_t'^2 \tag{33}$$

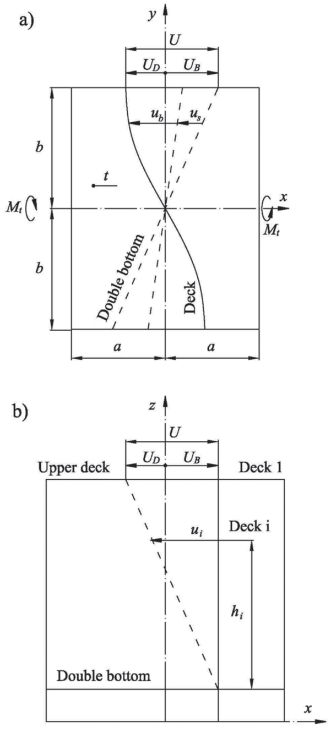

Figure 7. Upper deck deformation and double bottom rotation, a—bird view, b—lateral view.

On the other hand, total energy of the closed hull segment can be obtained by summing up energy of open segment and the deck strain energy, i.e.

$$E_{tot}^{*}=E_w^{\circ}+E_t^{\circ}+E_1-E_{\mu} \tag{34}$$

where

$$E_w^{\circ}=\frac{1}{2}\int_{-a}^{a}B_w^{\circ}\psi_t''\,\mathrm{d}x,\qquad E_t^{\circ}=\frac{1}{2}\int_{-a}^{a}T_t^{\circ}\psi_t'\,\mathrm{d}x,$$
$$E_{\mu}=\frac{1}{2}\int_{-a}^{a}\mu_x\psi\,\mathrm{d}x \tag{35}$$

Within a short span $2a$, constant value of ψ_t' (as for deck) can be assumed, so that second term in Eq. (35) by inserting T_t° from Eq. (10), leads to

$$E_t^{\circ}=GI_t^{\circ}a\psi_t'^2. \tag{36}$$

E_t° and E_1 in (34) can be unified into one term since both depend on $\psi_t'^2$

$$E_t^{\circ}+E_1=Ga\tilde{I}_t\psi_t'^2 \tag{37}$$

where

$$\tilde{I}_t = (1+C) I_t^{\circ}, \quad C = \frac{E_1}{E_t^{\circ}} \tag{38a,b}$$

$\tilde{I}_t$ is the effective torsional modulus which includes both open cross-section and deck effects.

Engine room structure is designed in such a way that the hold double skin continuity is ensured and necessary decks are inserted between the double skins. Strain energy is derived for the first (main) deck and for the others it can be assumed that their strain energy is proportional to the deck plating volume, V, and linearly increasing deformation with the deck distance from inner bottom, h, Figure 7, since the double bottom is much stiffer than decks. In that way the coefficient C, Eq. (38b), by employing (33) and (36), reads

$$C = \frac{\sum E_i}{E_t} = \frac{4(1+\nu) t_1 \left(\frac{a}{b}\right)^3 \left(|w_D| + |w_B|\right)^2 k}{\left[1 + 2(1+\nu)\left(\frac{a}{b}\right)^2\right] I_t^{\circ} a} \tag{39}$$

where

$$k = \sum \frac{V_i}{V_1} \left(\frac{h_i}{h_1}\right)^2. \tag{40}$$

In the above consideration distortion of cross-sections is not included and that is subject of further investigation.

4.2 *Torsion of segmented girder*

Couple of problems arise in the beam modelling of container ship structures: connection of closed parts, i.e., fore and aft peaks and engine room, with open holds and accounting for transverse bulkheads effect. Due to different vertical position of the shear centre, coupling between torsion and horizontal bending exists within displacements and sectional forces; $Y^* = Y^{\circ} + \psi\left(z_{SC}^* - z_{SC}^{\circ}\right)$, $T^{\circ} = T^* + Q\left(z_{SC}^* - z_{SC}^{\circ}\right)$ where Y is deflection, ψ is twist angle, T is torque and Q is shear force, z_{SC} is coordinate of shear centre. Warping compatibility in the joint of open and closed cross-section presents another problem which can be solved in the conventional or an advanced way, respectively:

a. Equilibrium of bimoments, B_w, and compatibility of twist angle derivatives, ψ'. Coupling between torsion and bending on the compatibility basis is avoided.
b. Discontinuity of twist angle derivatives $\psi'\left(x^+\right) = s_1 \psi'\left(x^-\right)$, and coupling between bending angles and twist angle $\varphi\left(x^+\right) = \varphi\left(x^-\right) + s_2 \psi'\left(x^-\right)$; equilibrium of bending moments $M\left(x^-\right) = M\left(x^+\right)$ and bimoments $B_w\left(x^-\right) = s_1 B_w\left(x^+\right) - s_2 M(x)$, where s_1 and s_2 are the warping compatibility factors which depend on warping function, (Haslum & Tonnessen, 1972, Pedersen, 1983).

Let us consider a girder consisting of three segments, Figure 8. The end segments are open and the middle one is closed, so that the girder is symmetric with respect to the z axis. Each segment is specified in its local coordinate system. The relevant expressions for displacements and sectional forces are listed below (Senjanović et al., 2009c):

$$\begin{aligned}
u &= w \frac{\mathrm{d}\psi_t}{\mathrm{d}x} = w\left(\frac{A_1}{l} + A_2 \alpha \mathrm{sh}\alpha x + A_3 \alpha \mathrm{ch}\alpha x + \psi_p'\right), \\
T_t &= GI_t\left(\frac{A_1}{l} + A_2 \alpha \mathrm{sh}\alpha x + A_3 \alpha \mathrm{ch}\alpha x + \psi_p'\right), \\
T_w &= -GI_t\left(A_2 \alpha \mathrm{sh}\alpha x + A_3 \alpha \mathrm{ch}\alpha x\right) - EI_w \psi_p''' s \\
T &= GI_t\left(\frac{A_1}{l} + \psi_p'\right) - EI_w \psi_p''', \\
B_w &= GI_t\left(A_2 \mathrm{ch}\alpha x + A_3 \mathrm{sh}\alpha x\right) + EI_w \psi_p'',
\end{aligned} \tag{41}$$

where ψ_p represents particular solution of differential equation and coefficient α yields

$$\alpha = \sqrt{\frac{GI_t}{EI_w}}. \tag{42}$$

Symbols A_i and B_i are used for integration constants of closed and open segment.

Compatibility coefficients s_1 and s_2 in the formulation (a) of compatibility conditions, specified in Introduction, depends on I_w^* and I_w° (Pedersen, 1983). Since I_w° instead of I_w^* is taken into account, $s_1 = 1$ and $s_2 = 0$. As a result, the torsion doesn't induce horizontal bending so that the conventional compatibility conditions (a) at the joint of closed and open segments can be used. Thus, the boundary and compatibility conditions in the considered case, yield

$$\begin{aligned}
&\psi^*(a) = \psi^{\circ}(0), \ \psi_t^{*\prime}(a) = \psi_t^{\circ\prime}(0), \\
&T^*(a) = T^{\circ}(0), \ B_w^*(a) = B_w^{\circ}(0), \\
&u^{\circ}\left(l^{\circ}\right) = 0, \ T^{\circ}\left(l^{\circ}\right) = M_t.
\end{aligned} \tag{43}$$

From the third and last conditions (43) one finds

$$A_1 = \frac{M_t a}{G\tilde{I}_t}, \ B_1 = \frac{M_t l^{\circ}}{GI_t^{\circ}}. \tag{44}$$

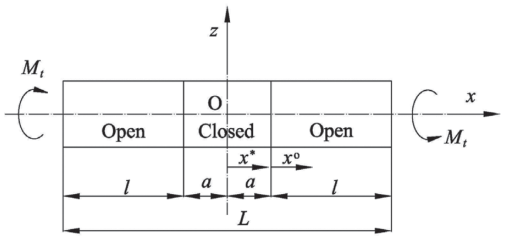

Figure 8. Torsion of segmented girder.

The remaining four conditions (43) lead to the following system of algebraic equations:

$$\begin{bmatrix} \alpha \mathrm{ch}\alpha a & 0 & -\beta \\ \tilde{I}_t \mathrm{sh}\alpha a & -I_t^\circ & 0 \\ 0 & \beta \mathrm{sh}\beta l^\circ & \beta \mathrm{ch}\beta l^\circ \end{bmatrix} \begin{Bmatrix} A_3 \\ B_2 \\ B_3 \end{Bmatrix} = \frac{M_t}{G} \begin{Bmatrix} \frac{1}{I_t^\circ} - \frac{1}{\tilde{I}_t} \\ 0 \\ -\frac{1}{I_t^\circ} \end{Bmatrix} \tag{45}$$

$$B_0 = A_1 + A_3 \left(1 - \frac{\tilde{I}_t}{I_s^\circ}\right) \mathrm{sh}\alpha a - B_2 \left(1 - \frac{I_t^\circ}{I_s^\circ}\right), \tag{46}$$

where

$$\alpha = \sqrt{\frac{G\tilde{I}_t}{EI_w^\circ}},\ \beta = \sqrt{\frac{GI_t^\circ}{EI_w^\circ}}. \tag{47}$$

The solution of system (45) reads

$$A_3 = \frac{D_{A3}}{D},\ B_2 = \frac{D_{B2}}{D},\ B_3 = \frac{D_{B3}}{D}, \tag{48}$$

where

$$\begin{aligned} D_{A3} &= \frac{M_t}{G}\left[\left(1 - \frac{I_t^\circ}{\tilde{I}_t}\right)\mathrm{ch}\beta l^\circ - 1\right], \\ D_{B2} &= -\frac{M_t}{G}\mathrm{sh}\alpha a\left[\left(1 - \frac{\tilde{I}_t}{I_t^\circ}\right)\mathrm{ch}\beta l^\circ + \frac{\tilde{I}_t}{I_t^\circ}\right], \\ D_{B3} &= \frac{M_t}{G}\left[\left(1 - \frac{\tilde{I}_t}{I_t^\circ}\right)\mathrm{sh}\alpha a\ \mathrm{sh}\beta l^\circ - \frac{\alpha}{\beta}\mathrm{ch}\alpha a\right], \\ D &= I_t^\circ \alpha \mathrm{ch}\alpha a\ \mathrm{ch}\beta l^\circ + \tilde{I}_t \beta \mathrm{sh}\alpha a\ \mathrm{sh}\beta l^\circ. \end{aligned} \tag{49}$$

5 HYDRODYNAMIC MODEL

Harmonic hydroelastic problem is considered in frequency domain and therefore one operates with amplitudes of forces and displacements. In order to perform structural and hydrodynamic coupling, it is useful to split total hydrodynamic force F^h into two parts: the first part F^R depending on the structural deformations, and the second one F^{DI} representing the pure excitation (Malenica et al., 2003). Furthermore, the modal superposition method is used. Vector of the wetted surface deformations $\mathbf{H}(x, y, z)$ can be presented as a series of dry natural modes $\mathbf{h}_i(x, y, z)$.

The potential theory assumptions are adopted for the hydrodynamic part of the problem and the total velocity potential φ, in the case of no forward speed, is defined with the Laplace differential equation and the given boundary values. Furthermore, the linear wave theory enables decomposition of the total potential (Malenica, 2003)

$$\varphi = \varphi_I + \varphi_D - i\omega \sum_{j=1}^{N} \xi_j \varphi_{Rj}, \quad \varphi_I = -i\frac{gA}{\omega} \mathrm{e}^{\nu(z+ix)}, \tag{50}$$

where φ_I is incident wave potential, φ_D is diffraction potential, φ_{Rj} is radiation potential and A and ω represent wave amplitude and frequency respectively. Once the potentials are determined, the modal hydrodynamic forces are calculated by pressure work integration over the wetted surface, S. The total linearised pressure can be found from Bernoulli's equation

$$p = i\omega\rho\varphi - \rho g z. \tag{51}$$

First, the term associated with the velocity potential φ is considered and subdivided into excitation and radiation parts

$$F_i^{DI} = i\omega\rho \iint_S (\varphi_I + \varphi_D)\mathbf{h}_i \mathbf{n}\, \mathrm{d}S, \tag{52}$$

$$F_i^R = \rho\omega^2 \sum_{j=1}^{N} \xi_j \iint_S \varphi_{Rj} \mathbf{h}_i \mathbf{n}\, \mathrm{d}S. \tag{53}$$

Thus, F_i^{DI} represents the modal pressure excitation. Now, one can decompose (53) into the modal inertia force and damping force associated with acceleration and velocity, respectively

$$F_i^a = \mathrm{Re}(F_i^R) = \omega^2 \sum_{j=1}^{N} \xi_j A_{ij},\ A_{ij} = \rho \mathrm{Re} \iint_S \varphi_{Rj}\, \mathbf{h}_i \mathbf{n}\, \mathrm{d}S, \tag{54}$$

$$F_i^v = \mathrm{Im}(F_i^R) = \omega \sum_{j=1}^{N} \xi_j B_{ij},\ B_{ij} = \rho\omega \mathrm{Im} \iint_S \varphi_{Rj}\, \mathbf{h}_i \mathbf{n}\, \mathrm{d}S. \tag{55}$$

where A_{ij} and B_{ij} are elements of added mass and damping matrices, respectively.

Determination of added mass and damping for rigid body modes is a well-known procedure in ship hydrodynamics. Now the same procedure is extended to the calculation of these quantities for elastic modes. The hydrostatic part of the total

pressure,—ρgz in (51), is considered within the hydrostatic model.

6 HYDROSTATIC MODEL

There are few solutions for restoring stiffness in the literature (Price & Wu, 1985, Newman, 1994, Huang & Riggs, 2000, Malenica, 2003). In this study consistent formulation of restoring stiffness is used (Senjanović et al., 2009a, b, 2011), and here only basic formulae are given.

The restoring stiffness consists of hydrostatic and gravity parts. Work of the hydrostatic pressure as the generalized force can be written in the form

$$F^h = -\rho g \iint_S \left[H_z + Z(\nabla \mathbf{H}) \right] \mathbf{H}\mathbf{n} \mathrm{d}S, \tag{56}$$

where ∇ is Hamilton differential operator, **H** is displacement vector, dS is differential of wetted surface, Z is its depth and **n** is unit normal vector. Stiffness is generally defined as a relation between incremental force and displacement, so it is determined from the variational equation

$$\delta F^h = -\rho g \iint_S \left[H_z + Z(\nabla \mathbf{H}) \right] \delta\mathbf{H}\mathbf{n} \mathrm{d}S. \tag{57}$$

Furthermore, the modal superposition method is used, and the variation is transmitted to modes, i.e., modal forces and displacements

$$\delta F^h = \sum_{j=1}^{N} \delta F_j^h, \quad \mathbf{H} = \sum_{j=1}^{N} \xi_j \mathbf{h}_j, \quad \delta\,\mathbf{H} = \sum_{j=1}^{N} \mathbf{h}_j \delta\xi_j. \tag{58}$$

In that way, Eq. (57) is decomposed into the modal equations

$$\delta F_i^h = -\sum_{j=1}^{N} \left[\left(C_{ij}^p + C_{ij}^{nh} \right) \xi_j \right] \delta\xi_i, \tag{59}$$

where

$$C_{ij}^p = \rho g \iint_S \mathbf{h}_i h_z^j \mathbf{n} \mathrm{d}S, \quad C_{ij}^{nh} = \rho g \iint_S Z \mathbf{h}_i \left(\nabla \mathbf{h}_j \right) \mathbf{n} \mathrm{d}S, \tag{60}$$

are stiffness coefficients due to pressure, and normal vector and mode contributions, respectively.

Similarly to the pressure part, the generalized gravity force reads

$$F^m = -g \iiint_V \rho_s \left(\mathbf{H}\nabla \right) H_z \mathrm{d}V, \tag{61}$$

where ρ_s and V are structure density and volume, respectively. By obtaining consistent variational equation and then by applying modal superposition method similarly as for hydrostatic part, the following modal variational equation is obtained

$$\delta F_i^m = -\sum_{j=1}^{N} C_{ij}^m \xi_j \delta\xi_i, \tag{62}$$

where

$$C_{ij}^m = g \iiint_V \rho_s \left(\mathbf{h}_i \nabla \right) h_z^j \mathrm{d}V, \tag{63}$$

are the gravity stiffness coefficients. Complete restoring stiffness coefficients are obtained by summing up its constitutive parts

$$C_{ij} = C_{ij}^p + C_{ij}^{nh} + C_{ij}^m. \tag{64}$$

7 HYDROELASTIC MODEL

After the definition of the structural, hydrostatic and hydrodynamic models, the hydroelastic model can be constituted. The governing matrix differential equation for coupled ship motions and vibrations is deduced

$$\left[\mathrm{k} + \mathrm{C} - i\omega(\mathrm{d} + \mathrm{B}(\omega)) - \omega^2 (\mathrm{m} + \mathrm{A}(\omega)) \right] = \mathbf{F}, \tag{65}$$

where **k**, **d**, and **m** are structural stiffness, damping and mass matrices, respectively, **C** is restoring stiffness, **B**(ω) is hydrodynamic damping, **A**(ω) is added mass, **ξ** is modal amplitudes, **F** is wave excitation and ω is encounter frequency. All quantities, except ω and ξ, are related to the dry modes. The solution of (65) gives the modal amplitudes ξ_i and displacement of any point of the structure obtained by re-tracking to (58).

8 NUMERICAL EXAMPLES

For the illustration of the procedure related to engine room effective stiffness determination, 3D FEM analysis of ship-like pontoon has been undertaken. The 3D FEM model is constituted according to 7800 TEU container ship. The complete hydroelastic analysis of the same ship has been performed.

8.1 *Particulars of the analyzed ship*

The main vessel particulars are the following:

Length overall L_{oa} = 334 m
Length between perpendiculars L_{pp} = 319 m
Breadth B = 42.8 m
Depth H = 24.6 m

Draught $T = 14.5$ m
Displacement, full load $\Delta_f = 135336$ t
Displacement, ballast $\Delta_b = 68387$ t
Engine power $P = 69620$ kW
Ship speed $v = 25.4$ kn.

The ship lateral plan is shown in Figure 9.

Stiffness properties of ship hull are calculated by program STIFF, based on the theory of thin-walled girders (Senjanović & Fan, 1992), Figure 10. The geometrical properties rapidly change values in the engine and superstructure area due to closed ship cross-section. This is especially pronounced in the case of torsional modulus, which takes quite small values for open cross-section and rather high for the closed one (Tomašević, 2007).

Influence of the transverse bulkheads is taken into account by using the equivalent torsional modulus for the open cross-sections instead of the actual values, i.e., $I_t^* = 2.4 I_t$. This value is applied for all ship-cross sections as the first approximation. The stiffness parameters of the bulkhead girders are listed in Tables 1 and 2, while the stool parameters are given in Table 3.

The bulkhead strain energy, determined according to formulae presented in Section 3 is given in Table 4.

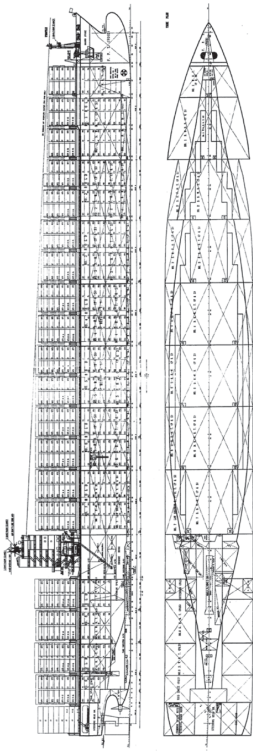

Figure 9. 7800 TEU container ship.

8.2 *Analysis of ship-like segmented pontoon*

Torsion of the segmented pontoon of the length $L = 300$ m, with effective parameters is considered. Torsional moment $M_t = 40570$ kNm is imposed at the pontoon ends. The pontoon is considered free in the space and the problem is solved analytically according to formulae given in Section 4. The reduction of torsional modulus of closed segment due to its shortness, i.e. deck contribution to torsional modulus of the open section, is elaborated in Section 4. The following values of the basic parameters are used: $a = 10.1$ m, $b = 19.17$ m, $t_1 = 0.01645$ m, $w_D = -221$ m^2, $w_B = 267$ m^2, $I_t^\circ = 14.45$ m^4, $k = 1.894$. As a result $C = 22.42$, Eq. (39), and accordingly $\tilde{I}_t = 338.4$ m^4, Eq. (38a), are obtained. Since $\tilde{I}_t = 0.36 I_t^*$, effect of the short engine room structure on its torsional stiffness is obvious.

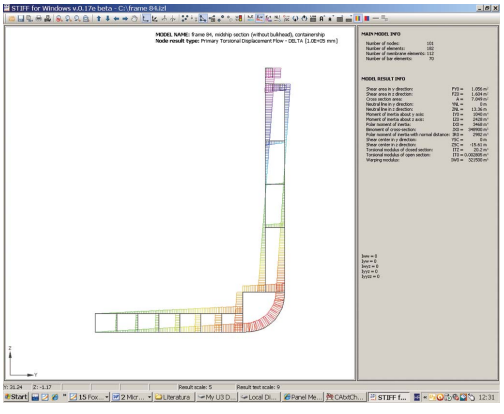

Figure 10. Program STIFF—warping of ship cross-section.

Table 1. Stiffness parameters of watertight bulkhead.

Girder	Moment of inertia I (m^4)	Tors. modulus I_t (m^4)	Spacing c (m)	Moment of inertia i (m^3)	Tors. modulus i_t (m^3)
Horiz.	0.02356	0.01555	2.6	0.00906	0.00493
Vert.	0.04196	0.03205	7.9	0.00531	

Table 2. Stiffness parameters of support bulkhead.

Girder	Moment of inertia I (m^4)	Tors. modulus I_t (m^4)	Spacing c (m)	Moment of inertia i (m^3)	Tors. modulus i_t (m^3)
Horiz.	0.00972	0.00486	2.6	0.00374	0.001696
Vert.	0.01944	0.01215	7.9	0.00246	

Table 3. Stool stiffness parameters.

Shear area A_s (m^2)	Moment of inertia I_s (m^4)	Tors. modulus I_{ts} (m^4)
0.45	0.07804	0.131

Table 4. Bulkhead strain energy, $U/(E\psi'^2)$.

Watertight bulkhead		Support bulkhead		Energy coefficient
Grillage (1)	Stool (2)	Grillage (3)	Stool (4)	C, Eq. (C5) (5) = [(1) + (2) + (3) + (4)]/2
29.691	28.872	12.051	28.872	49.743

The 3D FEM model of segmented pontoon is made by commercial software package SESAM and consists of 20 open and 1 closed superelement, Figures 11 and 12. The pontoon ends are closed with transverse bulkheads. The shell finite elements are used. The pontoons are loaded at their ends with the vertical distributed forces in the opposite directions, generating total torque $M_t = 40570$ kNm, Figure 13. The midship section is fixed against transverse and vertical displacements, and the pontoon ends are constrained against axial displacements (warping).

Lateral and bird view on the deformed segmented pontoon is shown in Figure 13, where the influence of more rigid engine room structure is evident. Detailed view on this pontoon portion is presented in Figure 14. It is apparent that segment of very stiff double bottom and sides rotate as a "rigid body", while decks and transverse bulkheads are exposed to shear deformation. This deformation causes the distortion of the cross-section, Figure 14.

Twist angles of the analytical beam solution and that of 3D FEM analysis for the pontoon bottom are compared in Figure 15. As it can be noticed, there are some small discrepancies between $\psi_{(1+2)D}$ and $\psi_{3D,bottom}$, which are reduced to a negligible value at the pontoon ends

Figure 15 also shows twist angle of side structure and the difference $\delta = \psi_{3D,bottom} - \psi_{3D,side}$ represents distortion angle of cross-section which is highly pronounced. As it is mentioned before, the problem will be further investigated.

8.3 *Validation of 1D FEM model*

The reliability of 1D FEM analysis is verified by 3D FEM analysis of the considered ship. For this purpose, the light weight loading condition of dry ship with displacement Δ = 33692 t is taken into account. The lateral and bird view of the first dominantly torsional mode of the wetted surface, determined by 1D model, is shown in Figure 16.

The first 3D dry coupled natural modes of the complete ship structure is shown in Figure 17, where Y and Z are vertical and transversal axis, respectively. It is similar to that of 1D analysis for the wetted surface. Warping of the transverse bulkheads, which increases the hull torsional stiffness, is evident.

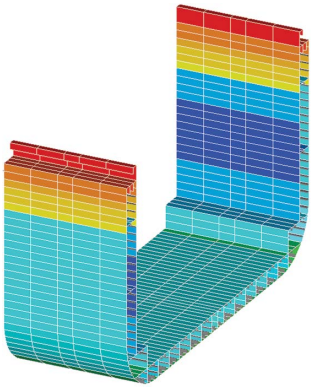

Figure 11. Typical superelement of open cross-section.

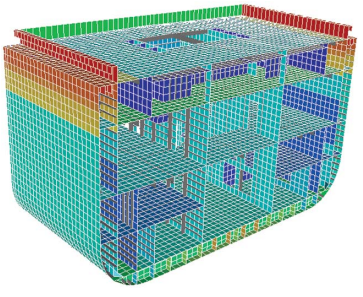

Figure 12. Engine room superelement.

Figure 13. Deformation of segmented pontoon, lateral and bird view.

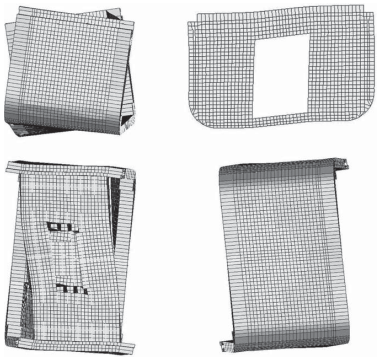

Figure 14. Lateral, axial, bird and fish views on deformed engine room superelement.

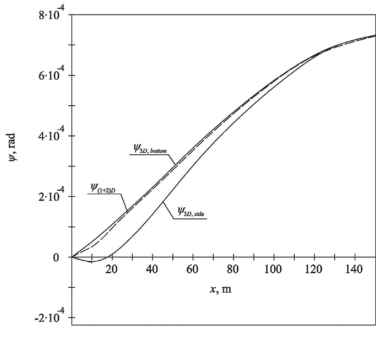

Figure 15. Twist angles of segmented pontoon.

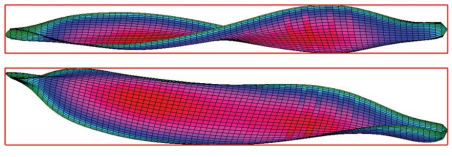

Figure 16. The first dominantly torsional mode, lateral and bird view, light weight, 1D model.

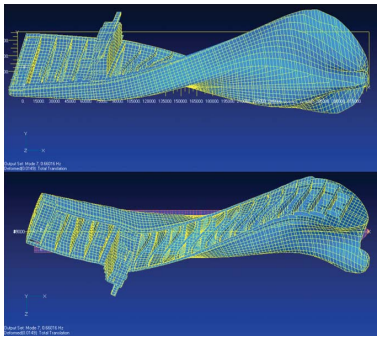

Figure 17. The first dominantly torsional mode, lateral and bird view, light weight, 3D model.

The first four corresponding natural frequencies obtained by 1D and 3D analyses are compared in Table 5.

Quite good agreement is achieved. Values of natural frequencies for higher modes are more difficult to correlate, since strong coupling between global hull modes and local substructure modes of 3D analysis occurs.

8.4 *Ship hydroelastic response*

Transfer functions of torsional moment and horizontal bending moment at the midship section are shown in Figures 18 and 19, respectively. They are compared to the rigid body ones determined by program HYDROSTAR. Very good agreement is obtained in the lower frequency domain, where the ship behaves as a rigid body. Discrepancies are very large at the resonances of the elastic modes, as expected.

Necessary condition for convergence of sectional forces to zero value as the wave frequency approaches to zero can be used as a benchmark for validation of the restoring stiffness.

Figure 20 shows the zoomed transfer function of torsional moment determined by the direct integration and three formulations of restoring stiffness in the hydroelastic approach: consistent one from this paper, symmetric matrix obtained by the minimum energy method, and hybrid matrix (Malenica, 2003). Only the consistent restoring stiffness satisfies the above condition as the rigid body solution does. In the case of symmetric and hybrid matrices the ship is not equilibrated. Moreover, the

Table 5. Dry natural frequencies, light weight, ω_i [rad/s].

	Vert.		Horiz. + tors.		
Mode no.	1D	3D	1D	3D	Mode no.
1	7.35	7.33	4.17	4.15	1(H0 + T1)
2	15.00	14.95	7.34	7.40	2(H1 + T2)
3	24.04	22.99	12.22	12.09	3(H2 + T3)
4	35.08	34.21	15.02	16.22	4(H3 + T4)

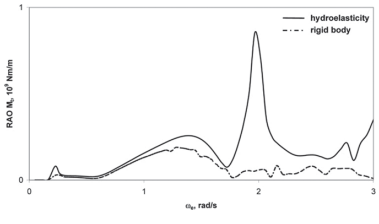

Figure 18. Transfer function of torsional moment, $\chi = 120°$, $U = 25$ kn, $x = 155.75$ m from AP.

consistent restoring stiffness emphasizes the roll resonance at 0.23 rad/s.

Shear influence on torsion is also investigated in the case of a pontoon with the cross-section equal to the midship section of the considered 7800 TEU container ship. One end of the pontoon is fixed and another is loaded with the concentrated torque. Calculation is performed analytically by employing the advanced beam theory and numerically by 3D FEM model. Rotation angles of the free pontoon end are shown in Figure 21.

Pure twist angle ψ_t is realized around the shear centre, S.C., and is somewhat smaller than the twist angle determined by 3D FEM model.

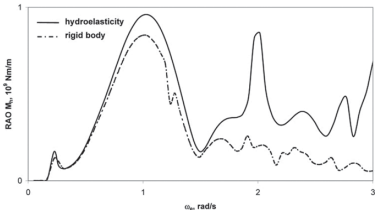

Figure 19. Transfer function of horizontal bending moment, $\chi = 120°$, $U = 25$ kn, $x = 155.75$ m from AP.

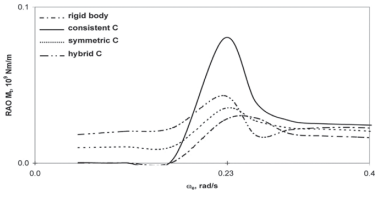

Figure 20. Zoomed transfer function of torsional moment, $\chi = 120°$, $U = 25$ kn, $x = 155.75$ m from AP.

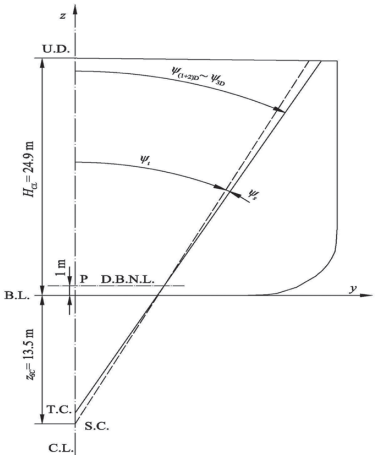

Figure 21. Twist angle at the pontoon end.

If the shear twist angle ψ_s is added to ψ_s around the double bottom centroid, value of the total twist angle approaches that of 3D analysis. As a result, the twist centre is determined, T.C.

9 CONCLUSIONS

Ultra large container ships are quite flexible so they stretch the bounds of present classification rules for appropriate structural design. Therefore, hydroelastic analysis has to be performed (Senjanović et al., 2008a, 2009a).

This paper represents an overview of the activities undertaken recent years to solve that challenging problem.

The illustrative numerical example of the 7800 TEU container ship shows that the developed hydroelasticity theory, utilizing sophisticated 1D FEM structural model and 3D hydrodynamic model, is an efficient tool for application in ship hydroelastic analyses. The obtained results point out that the transfer functions of hull sectional forces in case of resonant vibration (springing) are much higher than in resonant ship motion. Very good agreement between ship response determined by hydroelastic analysis and rigid body analysis in vicinity of zero frequency is obtained due to use of the consistent restoring stiffness.

The used advanced beam model of ship hull, based on advanced thin-walled girder theory with included shear influence on torsion and contribution of transverse bulkheads and engine room structure to its stiffness, is a reasonable choice for determining wave load effects. However, stress concentration in hatch corners calculated directly by the beam model is underestimated. This problem can be overcome by applying substructure approach, i.e., 3D FEM model of substructure with imposed boundary conditions from beam response. In any case, 3D FEM model of complete ship is preferable from the viewpoint of determining stress concentration.

In order to complete hydroelastic analysis of container ships and confirm its importance for ship safety, it is necessary to proceed further to ship motion calculation in irregular waves for different sea states, based on the known transfer functions. This includes determination of global wave loads, i.e., bending and torsional moments and their conversion into stresses, stress concentration in critical areas of ship structures, especially in hatch corners due to restrained warping, and fatigue of structural details.

At the end of a complete investigation, which also has to include model tests and full-scale measurements, it will be possible to decide on the extent of the revision of Classification Rules for

the design and construction of ultra large container ships.

REFERENCES

Bathe, K.J. 1996. *Finite Element Procedures*. Prentice Hall.

Bishop, R.E.D. & Price WG. 1979. *Hydroelasticity of Ships*. Cambridge University Press.

Haslum, K., Tonnessen, A. 1972. An analysis of torsion in ship hull. *European Shipbuilding* (5/6): 67–89.

Huang, L.L, & Riggs, H.R. 2000. The hydrostatic stiffness of flexible floating structure for linear hydroelasticity. *Marine Structures* 13: 91–106.

Kawai, T. 1973. The application of finite element method to ship structures. *Computers and Structures* (2): 1175–1194.

Malenica, Š. 2003. Some aspects of hydrostatic calculations in linear seakeeping. *Proc. 14th NAV Conf.*, Palermo.

Malenica, Š., Molin, B., Remy, F. & Senjanović, I. 2003. Hydroelastic response of a barge to impulsive and non-impulsive wave load. *Proc. Hydroelasticity in Marine Technology*, Oxford, 287–314.

Malenica, Š., Senjanović, I., Tomašević, S. & Stumpf, E. 2007. Some aspects of hydroelastic issues in the design of ultra large container ships. *Proc. IWWWFB*, Plitvice Lakes.

Newman, J.N. 1994. Wave effects on deformable bodies. *Applied Ocean Research* 16: 47–59.

Pavazza, R. 2005. Torsion of thin-walled beams of open cross-sections with influence of shear. *International Journal of Mechanical Sciences* 47: 1099–1122.

Pedersen, P.T. 1983. A beam model for the torsional-bending response of ship hulls. *RINA Transactions*: 171–182.

Pedersen, P.T. 1985. Torsional response of container ships. *Journal of Ship Research* 31: 194–205.

Price, W.G. & Wu, Y. 1985. *Hydroelasticity of Marine Structures*. In: Theoretical and Applied Mechanics, FI. Niordson & N. Olhoff, eds. Elsevier Science Publishers B.V.: 311–337.

Remy, F., Molin, B. & Ledoux, A. 2006. Experimental and numerical study of the wave response of flexible barge. *Proc. Hydroelasticity in Marine Technology*, Wuxi, 255–264.

Salvesen, N., Tuck, E.O. & Faltinsen, O.M. 1970. *Ship motion and sea loads*. Cambridge University Press.

Senjanović, I. 1998. *Finite Element Method in Ship Structures*. University of Zagreb, Zagreb, (in Croatian).

Senjanović, I. & Fan, Y. 1989. A higher-order flexural beam theory. *Computers & Structures* 32(5): 973–986.

Senjanović, I. & Fan, Y. 1992. A higher-order theory of thin-walled girders with application to ship structures. *Computers & Structures* 43(1): 31–52.

Senjanović, I. & Fan, Y. 1997. A higher-order torsional beam theory. *Engineering Modelling* 32(1–4): 25–40.

Senjanović, I. & Grubišić, R. 1991. Coupled horizontal and torsional vibration of a ship hull with large hatch openings. *Computers & Structures* 41(2): 213–226.

Senjanović, I., Malenica, Š., Tomašević, S. & Rudan, S. 2007. Methodology of ship hydroelastic investigation. *Brodogradnja* 58(2): 133–145.

Senjanović, I., Tomašević, S., Tomić, M., Rudan, S. & Vladimir, N. 2008a. Hydroelasticity of Very Large Container Ships. *Proc. Design and Operation Of Container Ships*, RINA, London, 51–70.

Senjanović, I., Tomašević, S., Rudan, S. & Senjanović, T. 2008b. Role of transverse bulkheads in hull stiffness of large container ships. *Engineering Structures* 30: 2492–2509.

Senjanović, I., Tomašević, S., Vladimir, N., Tomić, M. & Malenica, Š. 2009a. Ship hydroelastic analysis with sophisticated beam model and consistent restoring stiffness. *Proc. Hydroelasticity in Marine Technology*, University of Southampton, Southampton, 69–80.

Senjanović, I., Tomašević, S., Vladimir, N. & Malenica, Š. 2009b. Numerical procedure for ship hydroelastic analysis. *Proc. Intl. Conf. Computational Methods in Marine Eng.*, CIMNE, Barcelona, 259–264.

Senjanović, I., Tomašević, S. & Vladimir, N. 2009c. An advanced theory of thin-walled girders with application to ship vibrations. *Marine Structures* 22(3): 387–437.

Senjanović, I., Malenica, Š. & Tomašević, S. 2009d. Hydroelasticity of large container ships. *Marine Structures* 22(2): 287–314.

Senjanović, I., Tomašević, S., Vladimir, N., Tomić, M. & Malenica, Š. 2010. Application of an advanced beam theory to ship hydroelastic analysis. *Proc. Intl. Workshop on Advanced Ship Design for Pollution Prevention*, Taylor & Francis, London, 31–42.

Senjanović, I., Vladimir, N., Tomić, M. 2011. Formulation of consistent restoring stiffness in ship hydroelastic analysis. *Journal of Engineering Mathematics,* DOI: 10.1007/s10665-011-9468-2.

Szilard, R. 2004. *Theories and Applications of Plate analysis*. John Wiley & Sons, New York.

Tomašević, S. 2007. *Hydroelastic model of dynamic response of Container ships in waves*. Doctoral Thesis, University of Zagreb, Zagreb, (in Croatian).

Vlasov, V.Z. 1961. *Thin-Walled Elastic Beams*. Israel Program for Scientific Translation, Jerusalem.

Wu, J.S. & Ho, C.S. 1987. Analysis of wave induced horizontal and torsion coupled vibrations of ship hull. *Journal of Ship Research* 31(4): 235–252.